Applied Energy 269 (2020) 115150

Contents lists available at ScienceDirect

Applied Energy

journal homepage: www.elsevier.com/locate/apenergy

Experimental and numerical studies for applying hybrid solar chimney and photovoltaic system to the solar-assisted air cleaning system

Ming-Hua Huang[a], Lei Chen[a], Le Lei[a], Peng He[a], Jun-Ji Cao[c], Ya-Ling He[a], Zhen-Ping Feng[b], Wen-Quan Tao[a,*]

[a] Key Laboratory of Thermo-Fluid Science and Engineering of MOE, Xi'an Jiaotong University, Xi'an 710049, China
[b] Shaanxi Engineering Laboratory of Turbomachinery and Power Equipment, Xi'an Jiaotong University, Xi'an 710049, China
[c] Key Laboratory of Aerosol, SKLLQG, Institute of Earth Environment, Chinese Academy of Sciences, Xi'an 710061, China

HIGHLIGHTS

- Small test setups for both pure and hybrid solar chimney system are built.
- A numerical simulation method for the hybrid system is proposed and validated.
- Hybrid systems greatly increase the total power output.
- Hybrid systems can reduce land requirement of the solar-assisted air cleaning system.

ARTICLE INFO

Keywords:
Solar chimney
Photovoltaics
Air cleaning
Experiment
CFD

ABSTRACT

Under the background of global energy shortage and environment deterioration, researchers of the world pay high attention to develop renewable energy. This paper proposes a hybrid solar chimney and photovoltaic system for the novel solar-assisted air cleaning system. Small-scale laboratory setups are designed and fabricated. Experimental results reveal that replacing 50.60% acrylic glass of the collector top with photovoltaic panels will reduce the thermal air flow rate only by 14%, but generate significant electric power output. A three-dimensional numerical simulation model is established and validated by experimental results (air flow rate, temperature distribution). The model includes solar ray tracing model, surface to surface radiation model, buoyancy-driven flow and heat transfer model and power generation model. Then, this model is used to predict a large-scale system based on the Manzanares pilot power plant in Spain. For the large-scale system, the electrical energy generated by the photovoltaic panels can be used to drive suction fans to increase air input. Covering the entire top surface of the collector by photovoltaic panels (113-meter-wide), the total air flow rate would increase to 2.21 times compared with the system without photovoltaic panels. And setting photovoltaic panels on the collector bottom with 113-meter-wide, the total air flow rate would increase to 2.42 times. Thus, adding photovoltaic panels for the collector can greatly improve the utilization of solar energy. It can increase the amount of air purification, or reduce land requirement for the same flow rate.

1. Introduction

With the rapid development of economy, worldwide energy shortage and environmental pollution have become important factors restricting the sustainable development of human society. Moreover, energy production and use are by far the largest man-made sources of air pollutants [1]. Using renewable energy becomes the most promising means to overcome the shortage of fossil energy and the problem of environment deterioration. Solar energy as an inexhaustible green energy source in nature has attracted people's considerable attention. There are two main ways of solar power generation: one is solar thermal power generation, which converts solar radiation into heat, and then in some way to convert heat energy into electricity. The other is to convert solar energy directly into electrical energy without the thermal process, such as the photovoltaic effect. Compared high-temperature solar thermal power generation (such as concentrated solar thermal power generation), solar chimney power generation is a simple and low-temperature thermal power generation method with low

* Corresponding author.
E-mail address: wqtao@mail.xjtu.edu.cn (W.-Q. Tao).

https://doi.org/10.1016/j.apenergy.2020.115150
Received 5 March 2020; Received in revised form 30 April 2020; Accepted 4 May 2020
Available online 16 May 2020
0306-2619/

Nomenclature

Latin symbols

a	Thermal diffusivity, m^2/s
A	Area, m^2
c_p	Specific capacity, J/(kg·K)
g	Gravitational acceleration, m/s^2
G	Solar radiation, W / m^2
L	Length, m
N	Fan shaft power, kW
p	Pressure, Pa
Q	Source term, W/m^3; Flow rate, m^3/s
P	Power, W
R	Radius, m
Ra	Rayleigh number
T	Temperature, K
T_0	Operating temperature, K
U_i	Mean velocity component, m/s
x_i	The i^{th} Cartesian coordinate

Greek symbols

α	Absorptivity
β	Thermal expansion coefficient, 1/K
Δ	Difference
δ	Thickness, m
ε	Emissivity
η	Efficiency
ν	Kinematic viscosity, m^2 / s
ρ	Air density, kg / m^3
σ	Stefan-Boltzmann constant, $W/(m^2 \cdot K^4)$
τ	Transmittance

Subscripts

ave	Average
chimney	Chimney
fan	Fan
pv	Photovoltaic cell panel
ref	Reference value
turb	Turbine

investment and low operating cost. But the drawback of the solar chimney system is its low efficiency of solar energy utilization. Therefore, in the last decades solar chimney technology was often used in ventilation and grain drying. A few years ago, Cao et al. [2] proposed a solar-assisted large-scale cleaning system (SALSCS) for urban air remediation, which is a huge building covering an area of 19.63 square kilometers and with a 500 m high chimney. SALSCS is based on the principle of the solar chimney that solar energy is used to generate thermal airflow, which goes through filters to separate particulate matter (PM 10 and PM 2.5). Later such a smaller experimental cleaning system covering an area of 2580 square meters and with a 60 m high chimney has been constructed in Xi'an, China [3]. A picture and its schematic diagram are shown in Fig. 1. Due to the limitations of the solar chimney system, it needs very large urban area to collect enough solar energy for air purification. It is a well-known fact that urban land resources are very scarce. One possible way to significantly reduce area requirement for this kind of solar-assisted air cleaning system while still having a large enough air flow rate is to apply a hybrid solar chimney and photovoltaic (PV) system. PV panels not only generate electricity but also transfer heat to enhance rising thermal airflow. And the electric energy can be used to drive suction fans to enhance the air input to reduce the land requirement for the solar-assisted air cleaning system. Considering that the filter in Fig. 1 has a great impact on the system air input and its performance is greatly affected by the filter material, technology, and running time, as the preliminary study this paper does not take the filter into consideration. The major focuses of this study are three-folds. First to reveal the effect of covering part of the solar collector top surface by PV panels on the reduction of air flow rate going through the chimney by both numerical and experimental methods. Second to construct a reliable 3D efficient numerical model for simulating a hybrid solar chimney and photovoltaic system. Third to apply the constructed simulation model to study the air flow rate of large-scale system with PV panels covered in the solar-assisted air cleaning system.

In the following some previous related studies are briefly reviewed. The world's first solar chimney power plant with a 50 kW peak power capacity was built in Manzanares, Spain, in 1981, which had a chimney with a height of 194.6 m and a solar collector with a radius of 122 m [4]. Haaf presented preliminary test results of the pilot plant in 1984 [5]. Since then, some experiments of solar chimney system had been attempted. Zhou et al. [6] reviewed some small experiments. Gholamalizadeh and Mansouri [7] introduced Kerman pilot power plant in Iran. The radius of its solar collector was 20 m, the chimney was 60 m high and 3 m in diameter, and it could produce close to 400 Watts electrical power in solar insolation of 800 W/m^2. But due to the very low solar energy conversion efficiency, the commercialization of solar chimney system has not been achieved. Kasaeian et al. [8] suggested converting a simple solar chimney system into hybrids. Among the solar energy conversion systems that have been commercialized, the combination of the solar chimney system and the photovoltaic system is the most practical one. It is well-known that the photovoltaic power generation system has a much higher efficiency (more than 15%) than the solar chimney power generation system. However, PV panels generate both electricity and heat when exposed to sunlight [9]. The increasing temperature on the PV panel surface will reduce its efficiency and lower the output power. It is theoretically estimated that the output power of a crystalline solar cell will decrease by 0.4 – 0.5% when the temperature increase is equal to 1 °C above the optimum operating temperature [10,11]. PV panels can be cooled by air flow or water and the loss of power generation can be reduced. The waste heat of PV panels thus collected heats the air or water. This is PV-thermal (PVT) system which is a combined one where the PV not only generates electricity but also serves as a thermal energy supplier. PVT system is widely applied to the conventional solar water heater and passive building ventilation. Tonui and Tripanagnostopoulos [12] presented an air-cooled solar PVT system in a building. PV modules can be cooled by circulating air and the pre-heated air can be used for building thermal needs. In [13] a solar PVT system was compared with a pure solar hot water heater and a pure PV system. Results showed that the PVT system has higher utilization efficiency of solar energy than the pure solar hot water heater or the pure PV system. Chow [14] reviewed the PVT hybrid solar technology and pointed that benefited by the government policy and public awareness, the PVT technology has a large market and is expected to first become competitive with the conventional power generation. But all above applications are in traditional areas. Extending these technologies to other areas may improve their market competitiveness. In this paper, a new idea of applying the hybrid solar chimney and photovoltaic system to the field of air pollution control is put forward.

Numerical simulation method is a major method to study the solar chimney system and the PVT system. For the solar chimney system, Pastohr et al. [15] proposed a simplified 2D axisymmetric model. Since then, most numerical simulations of solar chimneys had used similar models [16–19]. This model takes into account the convection loss with

(a) Picture of SALSCS in Xi'an

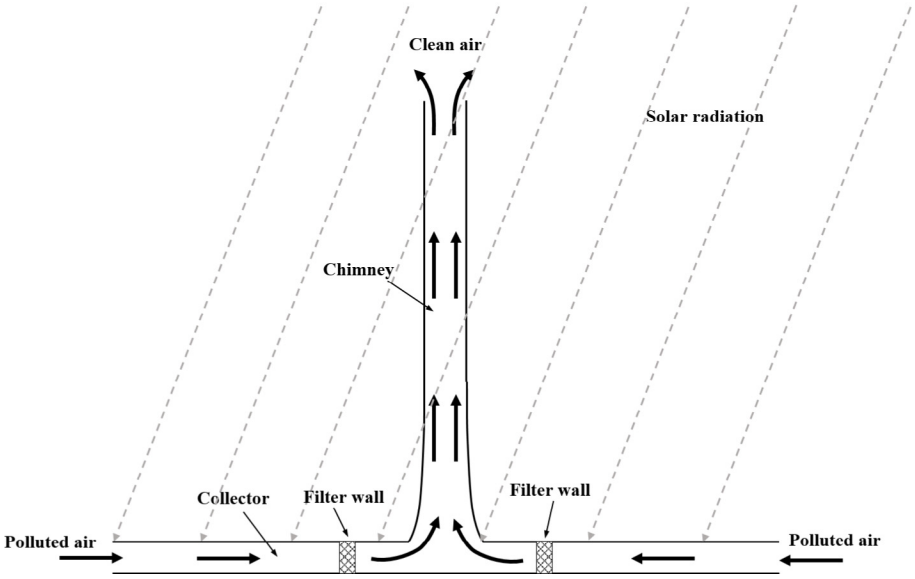

(b) Schematic of SALSCS

Fig. 1. Picture of SALSCS and its schematic diagram.

the ambient air and the heat storage loss of the soil layer, but the treatment of solar radiation is too simple. Solar radiation is only used as a heat source on the soil surface and the optical characteristics of the solar chimney system and the greenhouse effect in the solar collection are not considered. Greenhouse effect due to the radiation heat transfer inside the solar collector plays an important role in generating the upward buoyancy force. Gholamlizadeh and Kim [20] and Guo et al. [21] both simulated the Manzanares pilot power plant by a 3D model. In their simulations optical characteristics of the solar chimney system and the greenhouse effect in the solar collector were considered. The solar ray tracing model was adopted to simulate the incident solar radiation and the discrete ordinates (DO) radiation model was used to solve the radiative heat transfer equation. Their results revealed that accurately simulating the greenhouse effect is essential to correctly predict the performance of the solar chimney system. Huang et al. [22,23] proposed a simplified 2D radiation model for the collector based on the parallel infinite plates radiation model that could reflect optical characteristics of the solar chimney system and the greenhouse effect, and obtain consistent results with the 3D results of Gholamlizadeh and Kim [20] and the experiment data of the Manzanares pilot power plant [5]. This simplified model greatly saves computation time and computer sources. On this basis, Huang et al. [24] tried to combine the solar ray tracing model and the surface-to-surface (S2S) radiation model for a 3D case to simulate the solar chimney system that can be used for some inevitable 3D scenarios, like complex geometric configuration or uneven incident solar radiation. It is well-known that the general semi-transparent material such as glass has high transmittance for most solar radiation of $\lambda < 3\mu m$ and small transmittance for thermal radiation of $\lambda > 3\mu m$ [25]. DO radiation model can model this optical property of semi-transparent materials but it consumes much computation time. Although the S2S radiation model is based on gray-diffuse assumption, we can imagine that surfaces of semi-transparent materials are opaque to thermal radiation (in the infrared spectrum) and appear diffused. After solar ray tracing model simulating the solar rays passing through the semi-transparent surfaces, the S2S radiation model can be used to simulate the thermal radiation inside the solar chimney system

that will save computation time a lot than that of DO radiation model. For the simulation of photovoltaic systems, the key is to determine the PV electrical efficiency. An electrical efficiency model that efficiency varies linearly with the PV panel operating temperature is often used [26,27]. This electrical efficiency model can reflect the decrease in electrical efficiency with increasing panel temperature. Notton et al. [28] used a PV system connected to the electrical grid to verify this electrical efficiency model. They calculated the experimental photovoltaic electrical power on the basis of one month and compared it with the value estimated using this model. They found that the model was in a good accordance with the experimental data. Therefore, this paper also chooses this PV electrical efficiency model to predict PV panel power. Although many numerical simulations of solar chimney systems and photovoltaic systems have been done by researches, it should be noted that there are still some gaps in the existing numerical simulation research. One of the gaps is that a considerable amount of numerical simulation studies suffers from a lack of experimental validation [8]. In order to get reliable test data, we first set up a small-scale indoor test system to verify our proposed numerical model.

In this paper, we apply the hybrid solar chimney and photovoltaic system to the solar-assisted air cleaning system. A small-scale indoor test system including a laboratorial solar chimney system and a hybrid system is designed and built. And a numerical simulation method for the solar chimney system and the hybrid system is proposed and verified. Then a numerical model of the large-scale hybrid systems based on Manzanares pilot solar chimney power plant is constructed and the numerical simulations are performed. The system power output and air input are studied. The paper is organized as follows. A home-made laboratory setup including solar chimney and photovoltaic system (small-scale test systems) is described in Section 2. The physical and numerical models and the simulation methods are introduced in Section 3. The numerical models are presented, including solar ray tracing model, S2S radiation model, buoyancy-driven flow and heat transfer model and power generation model. Then, numerical simulation results of the small-scale tested systems and a large-scale system based on the Manzanares pilot solar chimney power plant are presented and discussed in Section 4. Finally, some conclusions are drawn in Section 5.

2. Experimental setup and procedure

We designed two indoor experimental setups. One is the pure solar chimney system and the other is the hybrid solar chimney and photovoltaic system. For the indoor experiments, xenon lamps are used as a solar radiation simulator, which create a solar-shining environment for the experiment study.

2.1. Experimental setup and measurement instruments

Fig. 2 shows the two experimental systems. System A is the pure solar chimney system and system B is the hybrid system. In order to avoid the environment wind influence, the two experimental systems are built in a closed test room made of rockwool sandwich panels and a toughened glass wall. Solar rays from a solar simulator enter the test room through the toughened glass wall and are absorbed by the system A or B. The solar simulator emits radiation in the spectrum of 0.3–2.5 μm and is set up in the simulator room separated from the test room by a wall of toughened glass. The wall of the simulator room is enclosed by rockwool sandwich panels and toughened glass. And in the solar simulator room, a series of extractor fans are used to take away the heated air from the solar simulator room to the outside ambient to prevent the solar simulator from overheating. A sensor (PTWD-2A) with radiation shield is used in the solar simulator room to monitor the environmental temperature and humidity. Four surface temperature sensors (PTWD-2A) are used to measure the temperature of the toughened glass wall.

As shown in Fig. 2 test systems A and B in the test room are placed on top of the test bed. The structure and dimensions of the systems A and B are shown in Fig. 3. For both systems the collector and chimney are made from 1 cm thick acrylic glass. The acrylic glass on the collector is tilted and supported by 3 cm × 3 cm square stainless-steel tubes. And the collector bottom is packed by the rubber insulation cotton. A low-pressure mass flow meter is embedded into the chimney. For system A, the diameter of the collecting is 260 cm, the total height of the chimney is 205.5 cm, and the inner diameter of the chimney is 8 cm. The height of collector inlet and outlet is 3.5 cm and 10 cm, respectively. The installation height of the mass flow meter is 60 cm from the entrance of the chimney. System B has the same dimensions as system A, but the top of its collector is covered by four monocrystalline silicon panels, which have dimensions of 81.6 cm × 80.6 cm and have a peak power output of 100 W. That means 50.60% top acrylic glass is replaced by photovoltaic panels.

Some calibrated Type-K thermocouples are used to monitor the temperature changes. Fig. 4 shows positions of thermocouples installed on the system A and B. There are six thermocouples to monitor the air temperature changes in the test system as shown in Fig. 4(a). Four thermocouples (T_1 to T_4) are placed at the circumference of the collector inlet and the remaining two thermocouples are set up at the chimney inlet and outlet, respectively. For the system A, the collector bottom absorbs most solar radiation and is the major monitoring object, and for the system B the PV panels absorb most solar radiation and are the major monitoring object. Figs. 4(b) and 4(c) show the thermocouple

(a) System A: the solar chimney system

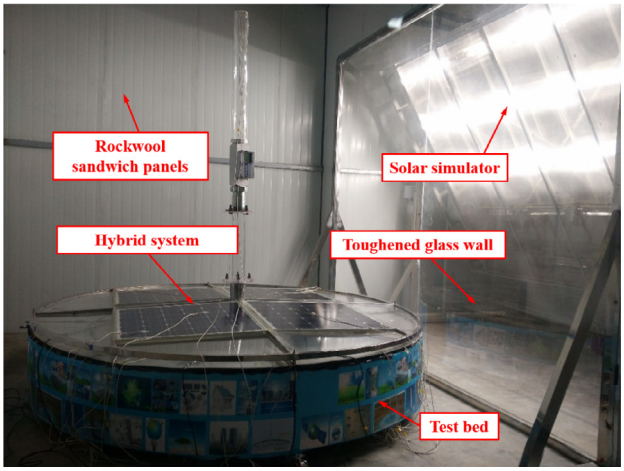

(b) System B: the hybrid solar chimney and photovoltaic system

Fig. 2. Photos of the experimental setups.

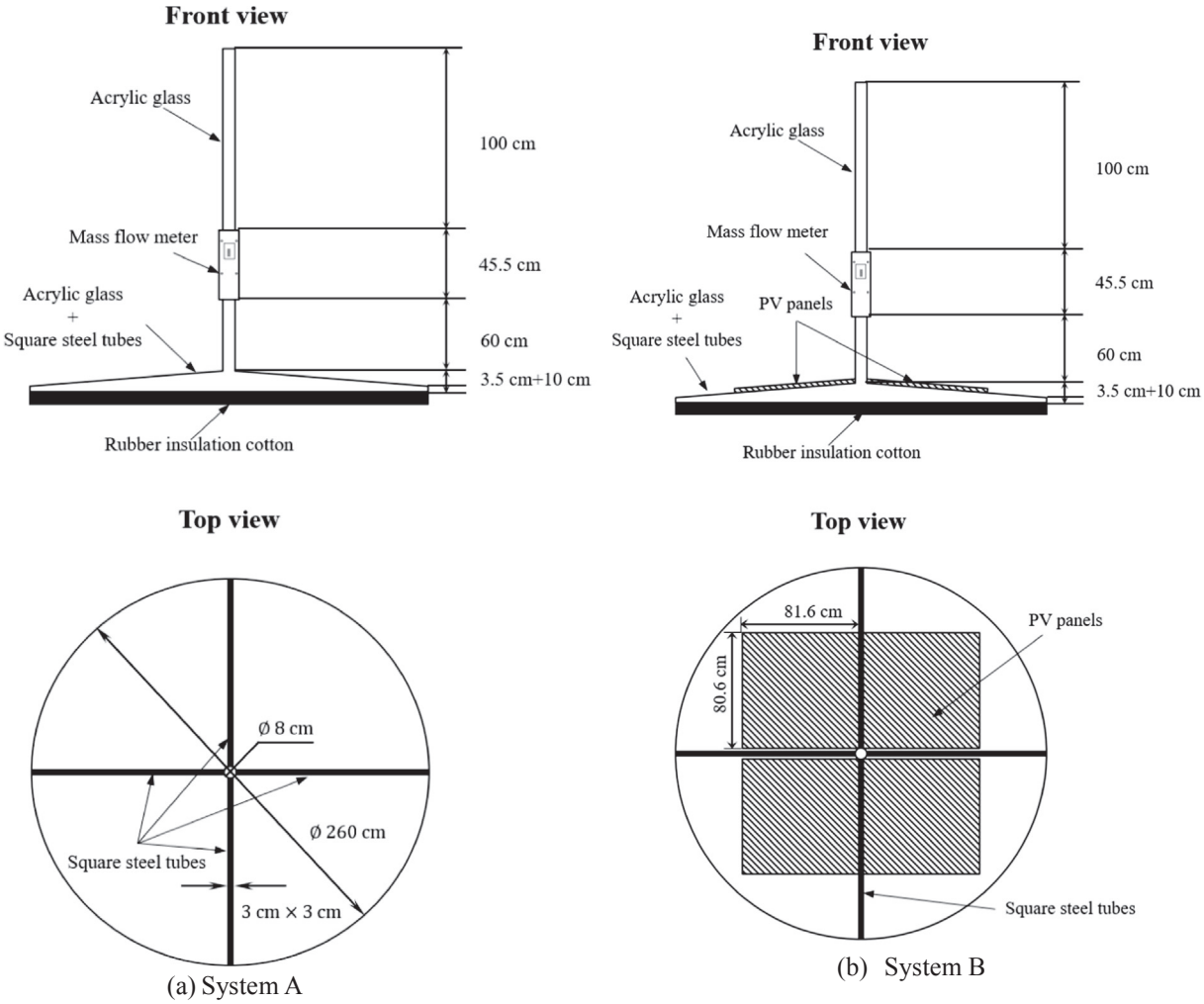

Fig. 3. The structure and dimensions sketch of the system A and B.

layout for monitoring the wall temperature changes.

The low-pressure mass flow meter (MF80GD-160) is used to monitor the air flow rate in the chimney whose readings are corrected to standard state (101.325 kPa, 20 °C) automatically. Four solar photovoltaic panels are connected in series and the voltage, current and electrical power are measured by a digital power meter. The irradiance of light reaching the toughened glass, passing through the toughened glass, reaching the surface of the acrylic glass and passing the acrylic glass is measured by the solar power meter (TBQ-2A). Hence the transmission rate of the toughened glass wall and the acrylic glass can be obtained.

2.2. Experimental procedure

To start the experiment, first tune on the extractor fans, then turn on the solar simulator power supply and adjust the angle between the solar simulator and the horizontal plane to 60-degree. Throughout the test process, in the solar simulator room the light source intensity and angle of the incident irradiation should be remained the same. In the test room, under the continuous shining of the simulator, the whole test system gradually tends to be in a steady state.

After turning on the extractor fans and xenon lamps successively, turn on the data monitoring instruments to monitor the system mass flow, temperature of monitoring points, wind speed of fans, equipment voltage, current and other parameters, and save the data every ten minutes. When the detected temperature variation is in the 1.0 degree range, the system is considered to be in a stable state. Usually it takes three hours to reach a steady sate. The measurement process usually lasts half an hour, during which three times of measurement are taken and the results are averaged. Once finishing the experiment, first turn off the xenon lamps and keep the fans running until the temperature of the solar simulator drops to the room temperature.

3. Numerical method

3.1. Mathematical formulation

Outdoor large-scale solar chimney system, like Manzanares pilot solar chimney power plant, converts solar radiation into heat and then generates thermal air to drive the wind turbine generator. The indoor test systems built in this paper are small in scale and cannot drive a wind turbine. However, the process of converting solar energy into internal energy of air is similar. In the small-scale test solar system and the hybrid system, when the solar light from the solar simulator meets the collector bottom it is converted to the thermal energy of the collector bottom, and when the light meets the PV panels it is converted to electric energy and thermal energy. The air within the collector is heated by the collector bottom or the back-side of PV panels and then started to move towards to the chimney under the action of buoyancy. As mentioned above, there are two differences between the tested small-scale systems and the outdoor large-scale system. One is that the small-scale systems have no turbine machine in the chimney, while in the large-scale system a turbine machine is positioned at the chimney inlet to convert the mechanical energy of the heated air into electricity. The other is that the collector bottom of the small-scale systems is

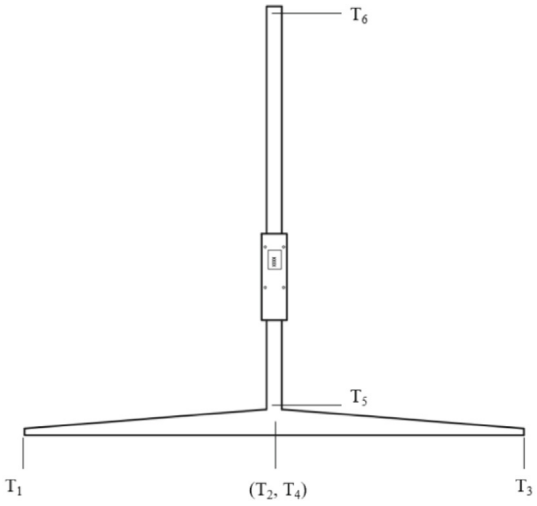

(a) Air temperature measurement points for system A and B (T_2 and T_4 at the circumference of the collector inlet)

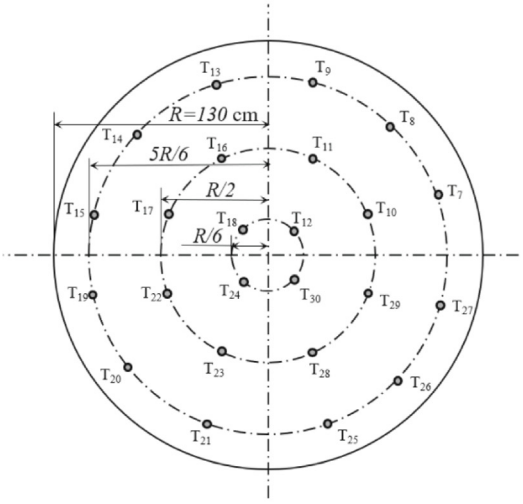

(b) Wall temperature measurement point at the collector bottom for system A

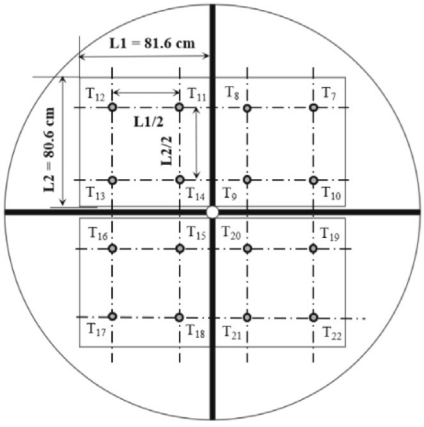

(c) Wall temperature measurement point at the collector top for system B

Fig. 4. Temperature measurement points for air and walls.

packed by the rubber insulation cotton, while the collector bottom of the large-scale system touches the ground, and some of the solar energy is stored in the soil layer.

According to the above-mentioned solar energy conversion process, the mathematical formulation includes the solar ray tracing model, the radiation model, the buoyancy-driven flow/heat transfer model and the power generation model.

3.1.1. Solar ray tracing model and radiation model

The ray tracing approach provided by FLUENT 14.0 is used to compute radiation effects of sun beams entering the computation domain. The ray tracing approach simulates the sun rays by the sun position vector and illumination intensity, and loads solar irradiation for boundary faces of the computation domain.

As stated in the introduction section, we can assume that surfaces of semi-transparent materials are opaque to thermal radiation, so the S2S radiation model can be used to compute the thermal radiation exchange between surfaces in the collector. The energy flux leaving a given surface consists of directly emitted and reflected energy, and can be expressed as [29]:

$$J_k = E_k + \rho_k \sum_{j=1}^{N} F_{kj} J_i \tag{1}$$

where, J_k represents the total radiative energy that is leaving surface k, and $E_k = \varepsilon_k \sigma T_k^4$ represents the emissive power of surface k, ρ_k is the reflectivity of surface k, and F_{kj} is the view factor between surface k and j. For N surfaces, Eq. (1) represents N equations. It is assumed that surfaces are diffuse and grey, so $\alpha_k = \varepsilon_k$, and $\rho_k = 1 - \varepsilon_k$.

3.1.2. Buoyancy-driven flow and heat transfer model

A buoyancy driven flow occurs in the solar chimney system and the hybrid system. The airflow is assumed incompressible and the Bossinesq approximation [30,31] is applied to simulate the buoyancy effect. The buoyancy driven flow is termed as natural convection flow and the strength can be measured by the Rayleigh number defined as follows:

$$R\,\mathrm{a} = \frac{g\beta\Delta T L^3}{\nu a} \tag{2}$$

where ΔT is the maximum temperature difference of the system, L is the characteristic length (for our case the collector height is taken as the characteristic length), and α is the air thermal diffusivity. Rayleigh numbers less than 10^8 indicates a laminar flow, and greater than 10^{10} indicates a turbulent flow. For the small-scale indoor test systems built in this paper, the Rayleigh numbers are all less than 10^8, however, for the large-scale systems based on Manzanares pilot solar chimney power plant the Rayleigh numbers are greater than 10^{10}. Therefore, the influence of turbulence is not considered when simulating the small-scale test systems, but is considered when simulating the large-scale systems.

For the small-scale indoor test systems, the steady conservation equations of the mass, momentum and energy of the air flow can be described as follows:

$$\frac{\partial U_i}{\partial x_i} = 0 \tag{3}$$

$$U_j \frac{\partial U_i}{\partial x_j} = -\frac{1}{\rho}\frac{\partial P}{\partial x_i} + \nu \frac{\partial^2 U_i}{\partial x_j \partial x_j} - g_i \beta (T - T_0) \tag{4}$$

$$U_j \frac{\partial T}{\partial x_j} = a \frac{\partial^2 T}{\partial x_j \partial x_j} + S_h \tag{5}$$

where ρ is the air density, ν is the kinematic viscosity, g is the gravitational acceleration, T is the local temperature, T_0 is the reference temperature, which is 25 °C for the small-scale systems, β is the thermal expansion coefficient equal to $1/T_0$, and S_h is volumetric heat sources.

For the large-scale systems, the standard k-ε turbulent model is adopted. The governing equations for the momentum and energy can be written as:

$$U_j \frac{\partial U_i}{\partial x_j} = -\frac{1}{\rho}\frac{\partial P}{\partial x_i} + \nu \frac{\partial^2 U_i}{\partial x_j \partial x_j} - \frac{\partial}{\partial x_j}(\overline{u_i' u_j'}) - g_i \beta (T - T_0) \quad (6)$$

$$U_j \frac{\partial T}{\partial x_j} = a \frac{\partial^2 T}{\partial x_j \partial x_j} - \frac{\partial}{\partial x_j}(\overline{u_j' T'}) + S_h \quad (7)$$

here the reference temperature T_0 is 300 K. The Reynolds stresses, $\overline{u_i' u_j'}$, and the heat flux, $\overline{u_j' T'}$, can be expressed as follows:

$$\overline{u_i' u_j'} = \frac{2}{3} k \delta_{ij} - \nu_t \left(\frac{\partial u_i}{\partial x_j} + \frac{\partial u_j}{\partial x_i} \right) \quad (8)$$

$$\overline{u_j' T'} = \frac{\nu_t}{\sigma_t} \frac{\partial T}{\partial x_j} \quad (9)$$

where k represents the turbulent kinetic energy, δ_{ij} represents the Kronecker delta, ν_t is the turbulent viscosity that can be expressed as $C_\mu k^2/\varepsilon$ in the standard k-ε turbulence closure, and $\sigma_t$is the energy Prandtl number as a model constant.

Transport equations for the turbulent kinetic energy, k and turbulent kinetic energy dissipation rate, ε can be described as

$$U_j \frac{\partial k}{\partial x_j} = \frac{\partial}{\partial x_j} \left[\left(\nu + \frac{\nu_t}{\sigma_k} \right) \frac{\partial k}{\partial x_j} \right] - \overline{u_i' u_j'} \frac{\partial u_i}{\partial x_j} + G_b - \varepsilon \quad (10)$$

$$U_j \frac{\partial \varepsilon}{\partial x_j} = \frac{\partial}{\partial x_j} \left[\left(\nu + \frac{\nu_t}{\sigma_\varepsilon} \right) \frac{\partial \varepsilon}{\partial x_j} \right] - C_{\varepsilon 1} \frac{\varepsilon}{k} (\overline{u_i' u_j'} \frac{\partial u_i}{\partial x_j} + C_{\varepsilon 3} G_b) - C_{\varepsilon 2} \frac{\varepsilon^2}{k} \quad (11)$$

here G_b is the contribution to the production of k and ε due to buoyancy that can be expressed by Eq. (12), and$C_{\varepsilon 3}$denotes the effect of the buoyancy on ε and is given by Eq. (13), where v is the component of the flow velocity parallel to the gravitation vector and u is the component of the flow velocity perpendicular to the gravitational vector [29].

$$G_b = \beta g_i \frac{\nu_t}{\sigma_t} \frac{\partial T}{\partial x_i} \quad (12)$$

$$C_{\varepsilon 3} = \tanh \left| \frac{v}{u} \right| \quad (13)$$

The model constants $C\mu$, $C_{\varepsilon 1}$, $C_{\varepsilon 2}$, σ_k, σ_ε and σ_t are specified as 0.09, 1.44, 1.92, 1.0, 1.3 and 0.85 [29,30].

For the large-scale systems, the heat transfer in the soil layer should be considered, and the temperature are governed by:

$$\frac{\partial^2 T}{\partial x_j \partial x_j} = 0 \quad (14)$$

3.1.3. Power generation model

The power output of the wind turbine and PV panels is determined as follows. A wind turbine converts the wind kinetic energy to the electric energy. The power output of the wind turbine can be expressed as [32,33]:

$$P_{turb} = \frac{1}{2} \eta_{turb} \rho A_{chimney} V_{ave}^3 \quad (15)$$

where V_{ave} is the average flow velocity at the turbine, $A_{chimney}$ is the turbine flow area, and η_{turb} represents the efficiency of the wind turbine.

The electrical power output of the PV panels depends on the temperature of the PV panels and can be written as follows [26–28,34]:

$$P_{pv} = G A_{pv} \eta_{ref} [1 + \beta_{ref} (T_{pv} - T_{ref})] \quad (16)$$

where η_{ref} is the reference efficiency at reference condition (irradiance 1000 W/m^2, PV panel temperature 25 °C), β_{ref} is the temperature coefficient that varies for different PV cell materials (about −0.3 to −0.45%/K for crystalline silicon, and −0.2 to −0.35%/K for thin film types technologies) [34]. In this paper β_{ref} takes a value of −0.35%/K, and η_{ref} is assumed 16% that is available for most commercial PV panels.

3.2. Boundary conditions of the two models

3.2.1. Small-scale model

The physical model and computational domain are shown in Fig. 5. The whole test room is the computation domain. The solar radiation from the solar simulator reaches the toughened glass wall with an average intensity of 689 W/m^2, and the transmittances of the toughened glass wall and the acrylic glass of the test systems are 0.50 and 0.92, respectively. The measured temperature of the toughened glass wall is applied as its boundary condition. The other walls of the test room are insulated with the rockwool and adiabatic boundaries are used. Ignoring the energy loss from the ground surface to the soil, the ground surface adopts adiabatic boundary. The collector bottom and lateral walls of the test bed also take adiabatic boundary condition. The collector top and chimney surface are interior wall in the computation domain, hence no boundary conditions are needed. However, for the

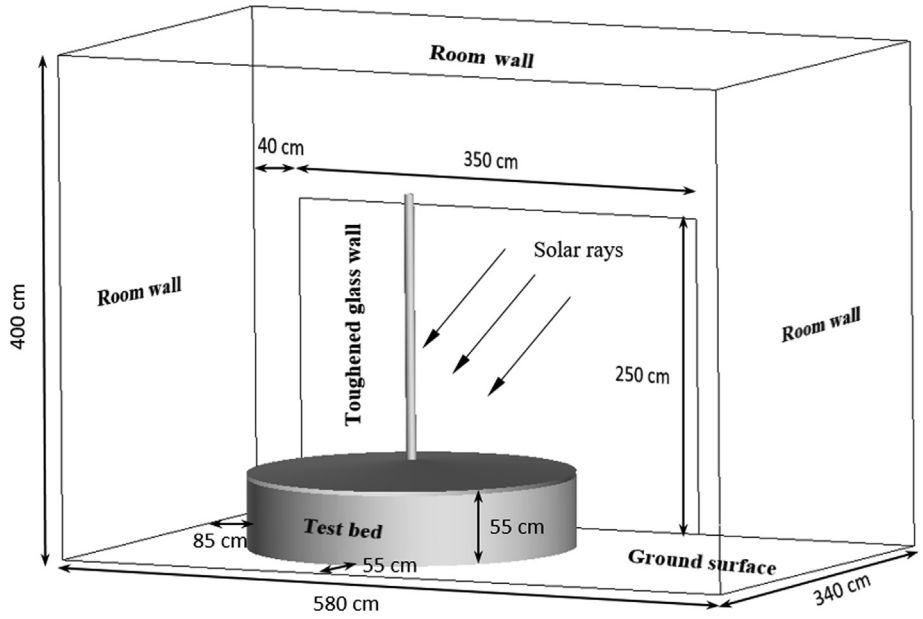

Fig. 5. Physical model for the indoor test systems.

hybrid test systems, to correctly deal with the term of generated electrical energy of the PV panels, the heat balance of the PV panels covering the collector top should be considered, which can be described as follows:

$$Q_{pv,solar} = Q_{pv,air} + Q_{pv,bottom} + Q_{pv,e} + Q_{pv,wall} + Q_{elec} \quad (17)$$

where $Q_{pv,solar}$ is the solar irradiation received by the PV panels per unit volume, which is computed by the solar ray tracing model. $Q_{pv,air} = h_{pv,air}(T_{pv} - T_{air})/\delta_{pv}$, is the convection heat flux between the bottom surfaces of PV panels and the air inside the collector. $Q_{pv,bottom}$ is the radiation heat flux between the bottom surfaces of PV panels and the bottom surface of the collector, which is calculated by the S2S model. $Q_{pv,e} = h_{pv,e}(T_{pv} - T_e)/\delta_{pv}$, is the convection heat flux between the top surfaces of PV panels and the environment. $Q_{pv,wall}$ is the radiation heat flux between the top surfaces of PV panels and the walls of the test room, which is calculated by the S2S model. And Q_{elec} represents the energy loss due to power generation of PV panels. In numerical simulation this term is treated as a negative heat source of the PV panels and expressed by Eq. (18).

$$Q_{elec} = -\frac{P_{pv}}{A_{pv}\delta_{pv}} \quad (18)$$

where P_{pv} takes the measured power output of the PV panels of 20 W.

3.2.2. Large-scale model

The physical model is three-dimensional based on the Manzanares pilot power plant and is indicated by two-dimensional axisymmetric picture in Fig. 6. The symbol "*L*" in Fig. 6 shows the width of the PV panels placed along the collector radius from its inlet. When $L = 0$ means the system is a pure solar chimney system.

A solid region with 5 m thick is used to represent the soil layer. The bottom wall temperature of the soil layer is set to be 300 K which was adopted by some previous simulations [15–24]. The ground surfaces at the collector bottom are coupled walls. Considering the convection with the environment and radiation to the sky, the top surfaces of the collector, including semi-transparent materials and PV panels are set as mixed wall boundary conditions of FLUENT. The convective heat transfer coefficient is taken as 4 W/(m^2·K) and the radiation emissivity to the sky is 0.8. For the large scale systems, the heat balance of the PV panels at the collector top and bottom can be expressed as Eq. (19) and Eq. (20), respectively.

$$Q_{pv,solar} = Q_{pv,air} + Q_{pv,bottom} + Q_{pv,e} + Q_{pv,\mathrm{sky}} + Q_{elec} \quad (19)$$

$$Q_{pv,solar} = Q_{pv,air} + Q_{pv,\mathrm{top}} + Q_{pv,soil} + Q_{elec} \quad (20)$$

where $Q_{pv,sky} = \varepsilon_{pv}\sigma(T_{pv}^4 - T_{sky}^4)/\delta_{pv}$, is the radiation heat flux between the top surfaces of PV panels and the sky, and ε_{pv} is equal to 0.8. $Q_{pv,\mathrm{top}}$ is the radiation heat flux between the top surfaces of PV panels and the top surface of the collector, which is calculated by the S2S model. $Q_{pv,soil}$ is the heat flux through the heat conduction into the soil layer. Q_{elec} is the negative source term considering the generated electricity and is determined by a user-defined function (UDF) according to Eq. (18), where the power output of the PV panels, P_{pv} is calculated by Eq. (16).

The pressure inlet condition and the pressure outlet condition are applied on the inlet and outlet of the fluid computation domain. Lateral boundaries of the soil layer and the alternator cover are adiabatic

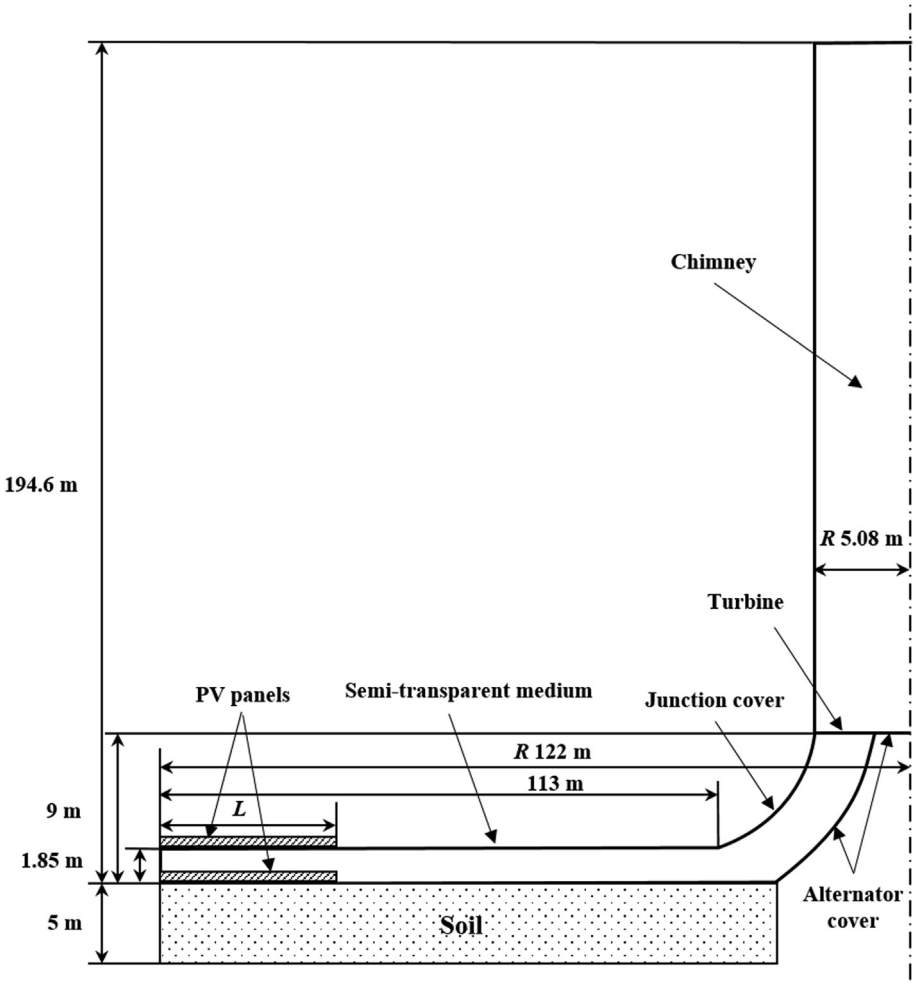

Fig. 6. The structure and dimensions sketch for the large-scale model based on Manzanares pilot power plant.

boundaries. For the full-load state of the wind turbine, a fan condition of FLUENT is employed to the wind turbine, and the pressure drop is calculated by Eq. (21), where P_{turb} is determined by Eq. (15). For the no-load state of the wind turbine, the interior boundary of FLUENT is used for the turbine.

$$\Delta p_{turb} = \frac{P_{turb}}{Q} \tag{21}$$

The midday solar radiation environment is simulated. The value of the solar radiation that enters through the semi-transparent collector into the computational domain is set as 850 W/m^2 with an incident angle of 90-degree, and the solar radiation transmittance of the semi-transparent surfaces is 0.92.

3.3. Numerical methods

For the small-scale indoor test systems, the solar ray tracing algorithm simulates the rays from the solar simulator to the experimental setups and laminar flow model is employed. For the large-scale systems, the solar ray tracing model is adopted to predict the incident energy form the sun, the steady RANS equations with standard k-ε turbulence closure and standard wall functions are used. For these two simulations, Boussinesq approximation is applied. The SIMPLE algorithm is applied, the second-order upwind discretization scheme is selected for convection term and the central difference discretization schemes is used for diffusion term. The mesh independence of numerical solutions is examined. For the small-scale system, the node number is 1.796×10^6. For the large-scale system the node number is 3.948×10^6, and the distance from the first layer grids to the wall is sufficiently small to guarantee that the Y^+ is in the range of 30 to 300.

4. Results and discussion

In this section, the numerical results of the small-scale test systems are first presented and compared with our test results to verify the reliability of our numerical simulation model. Then the numerical results of the large-scale systems are provided with detailed discussion and analyses.

4.1. Small-scale test systems

The small-scale solar chimney system doesn't have the ability to generate electric energy and the hybrid system with same dimensions only generates about 20 W electric energy by PV panels. So, the major aim of our experiments is to compare the system volumetric flow rate between the system A and the system B and verify the numerical model.

The measured values of the system volumetric flow rate are 8.768 Nm^3/h and 7.534 Nm^3/h (at the standard environmental conditions 101.325 kPa, 20 °C) for the systems A and B, respectively. The corresponding numerically predicted values are 8.691 Nm^3/h and 7.672 Nm^3/h, respectively, and the relative deviations of numerical values to measured values are 0.88% and −1.83%, respectively. Experimental results and numerical results are in good agreement and both reveal that the hybrid system has a bit lower volumetric flow rate due to replacing part acrylic glass with PV panels. The system volumetric flow rate of the hybrid system decreases only by 14% and 10% of the test data and the simulation results, respectively. Considering that half top surface of the collector is replaced by PV panels the amount of 10–14 percentage reduction in flow rate is very cost-effective.

Fig. 7 shows the distribution of solar heat flux on the bottom of the collector of systems A and B. It can be found that, due to the incidence of light at 60°and the shielding of the stainless-steel tubes and the PV panels, the solar flux at the bottom of the collector is not uniform. In addition, for system B, the bottom of the collector receives not too much solar radiation, so the heat flow generated by the system should mainly come from the heat dissipation of PV panels.

Fig. 8 shows the comparison of temperatures between experimental results and numerical results. The positions of the measured points of air temperature and wall temperature for the system A and B are indicated in Fig. 4. It can be seen that all predicted values show good agreement with measurements and the deviations between measurements and predicted values are within acceptable limits. Here the deviation is measured by the root mean square error (RMSE) defined as follows:

$$\mathrm{RMSE} = \sqrt{\frac{1}{n}\sum_1^n (c_o - c_p)^2} \tag{22}$$

here c_o refers to the observed value, c_p represents the simulation value, n is the number of monitors. The RMSE values is 1.99 °C and 1.90 °C for systems A and B, respectively.

The above validations by air flow rate and temperature distribution results show that the constructed numerical model can well predict the performance of the solar chimney system and the hybrid system.

4.2. Large-scale systems

In the numerical simulation of the large-scale system, three variants are studied: the first one is the solar chimney system without PV panels, that is, the Manzanares pilot SCPP which is simulated for further validating our numerical model, the second one is the hybrid system with

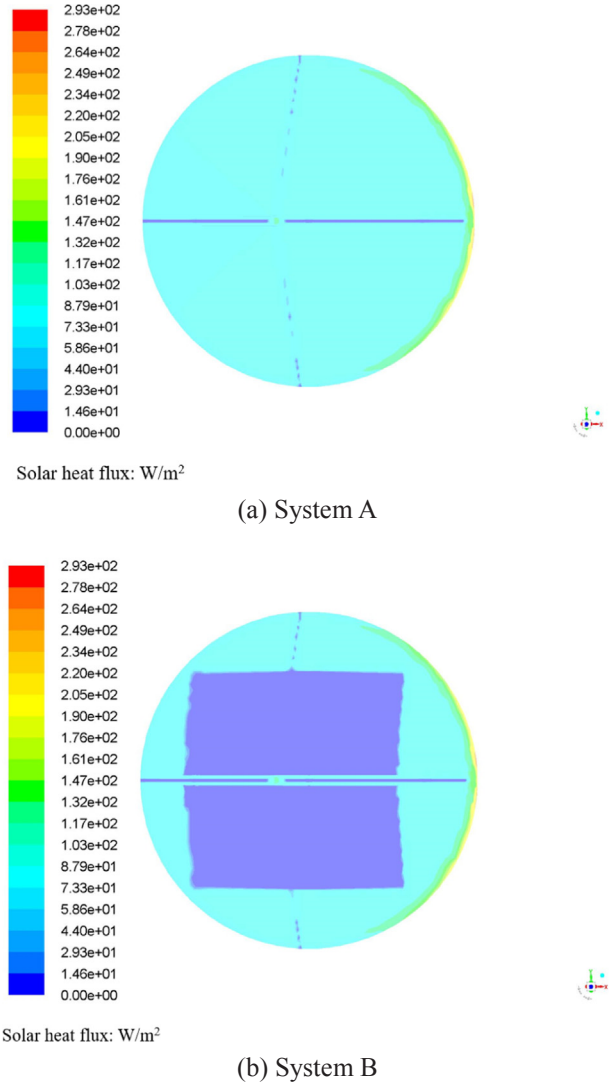

Fig. 7. The distribution of solar heat flux on the bottom of the collector.

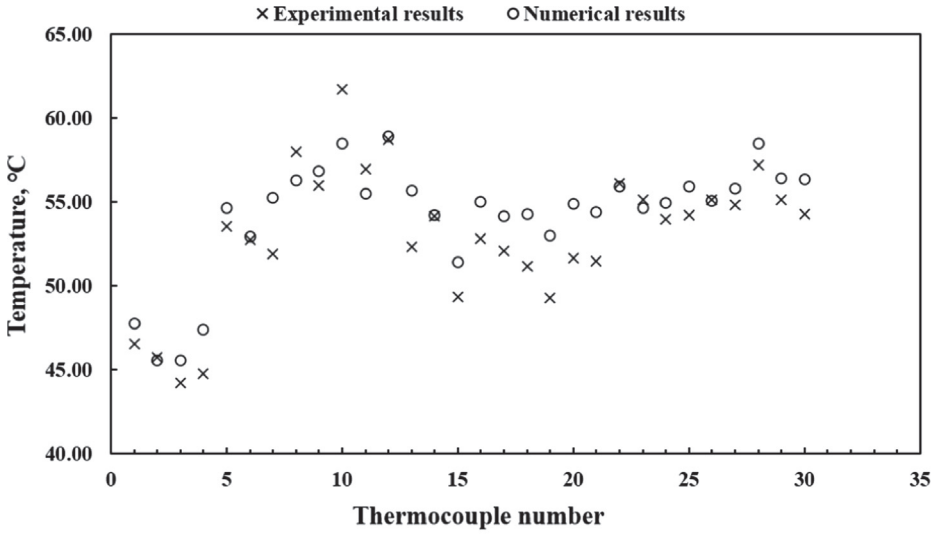

(a) System A

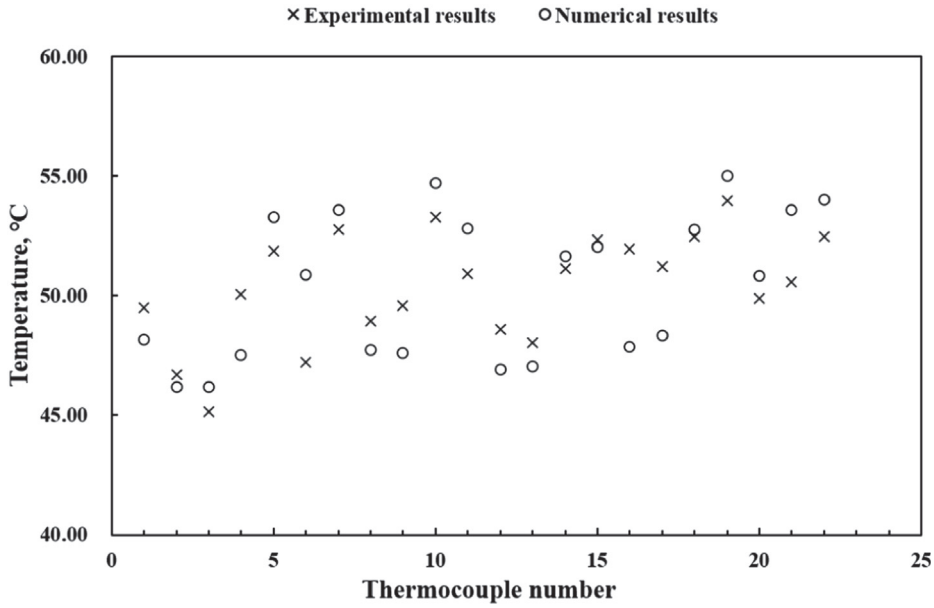

(b) System B

Fig. 8. Comparison between experimental results and numerical results.

PV panels at the top of the collector and the third one is the hybrid system with PV panels at the bottom of the collector. In this section, numerical results of the three variants are presented and compared.

First, the numerically simulated results of the Manzanares pilot SCPP are compared with the measurements. At 850 W/m^2 irradiation, the air temperature difference between the collector inlet and outlet and the potential power output given by Haaf [5] are 17.5 K and 48 kW, respectively. And the corresponding results by the present simulation are 18.76 K and 48.34 kW, respectively. So, the predicted values agree with the experimental data very well, once again showing the reliability of the constructed numerical model.

In the following, the simulation results of the three variants (systems) are presented and discussed.

(1) Influence of PV panels position

The three compared systems are denoted by without PV, with PV at bottom and with PV at top and $L = 40$ m is used for the latter two systems. Fig. 9 compares the volumetric flow rate for the three systems. As expected, the hybrid systems reduce the system volumetric flow rate, but not very much. The system volumetric flow rate is decreased by 3% and 19% for the system with PV at bottom and with PV at top, respectively. Accordingly, the turbine power output of the hybrid system converted from the airflow kinetic energy would decrease correspondingly, however, the system total power output would significantly increase contributed by the PV panels. Fig. 10 shows the turbine and PV power output. Compared with the solar chimney system, the system total power output of the two hybrid systems increases by 53 times and 57 times, respectively. The hybrid system with PV panels at the top of the collector generates the maximum electric power output. Because PV panels at the top of the collector has better heat dissipation. In addition

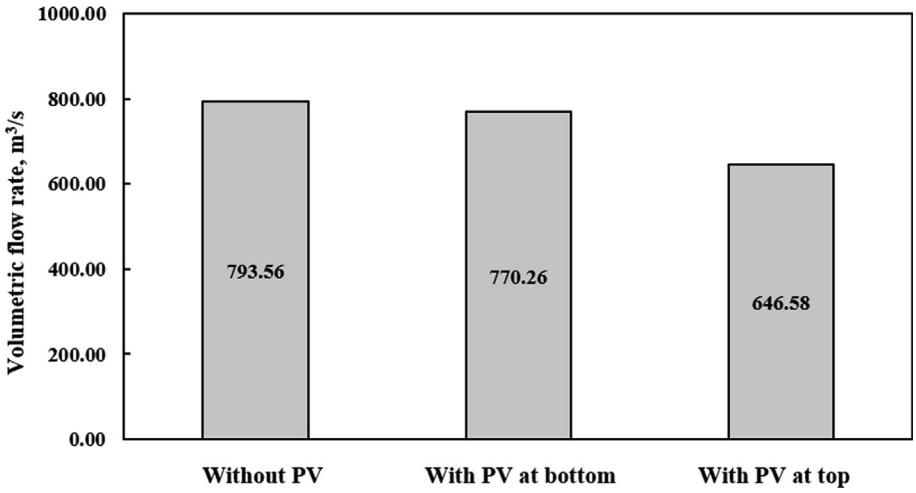

Fig. 9. Comparison of the system thermal volumetric flow rate when $L = 40$ m.

to the heat dissipation from the top of PV panels to the environment, the air flow underneath PV panels also makes forced convection cooling. For PV panels at the bottom of the collector, the air flow of the collector cools the top surfaces of PV panels, the bottom surfaces of the PV panels are in contact with the ground, and part of the heat is transferred to the soil layer. The predicted average temperature of the PV panels at top and at bottom are 50.01 ˚C and 67.32 ˚C, respectively. So, the electrical efficiency of the top PV is better than that of the bottom PV. However, when PV panels are at the collector top, the temperature of the ground surface shielded by the PV panels averaged is only 39.93 ˚C, which releases less heat to the air flowing over it than the system with PV panels at the collector bottom. That's why the thermal volumetric flow rate is greater when PV panels at bottom than PV panels at top.

For the solar-assisted air cleaning system, filter walls and other purification devices need to be installed in the collector, and some maintenance work also requires personnel to enter into and exit from the collector, so the arrangement of PV panel at bottom may not be very convenient. So, it is likely that placing the PV panels at the top of the collector of the solar-assisted air cleaning system should be recommended. In the following, discuss is focused on the second system.

(2) Influence of PV panels area

The hybrid systems with PV panels at the top of the collector are simulated. As shown in Fig. 6, $L = 113$ m denotes the whole collector canopy is covered by PV panels. Fig. 11 shows the volumetric flow rate with different L. The system volumetric flow rate decreases with the increase of the PV panels area. The system volumetric flow rate of $L = 40$ m, 80 m, and 113 m is 81.48%, 67. 01% and 60.71% of the pure solar chimney system, respectively. Fig. 12 shows the turbine and PV power output. The turbine power output decreases and the total power output increases with the increase of the PV panels area. Comparing the solar chimney system, the hybrid system total power output increases about 57 times, 91 times and 103 times for $L = 40$ m, $L = 80$ m and $L = 113$ m, respectively.

From above results it can be seen that by covering the top surface of the collector with PV panels even though the thermal volumetric flow rate of air reduces about 40%, but the power output can increase 100 times which can be used to drive a fan for suction of air from the environment. Thus from view point of solar-assisted air cleaning system it is interest to compare how much total air flow can be generated through such hybrid system. In the following presentation such comparison will be presented.

(3) Effect of PV panels on the air flow rate of the solar-assisted air cleaning system

For the solar-assisted air cleaning system, the system polluted air input is the key point. The solar chimney system without wind turbine will produce a greater system flow rate. Thus, the situations with turbine (termed full-load state) and without turbine (termed no-load state) are both simulated and compared. Our comparison focuses on how much air flow rate can be created by the electric power generated by the systems at the midday state. Taking into account the loss of direct current to alternating current, inverter efficiency, environmental loss and other losses, we assume 80% of the system's generated electricity, including the turbine power output and the PV power output, is used to

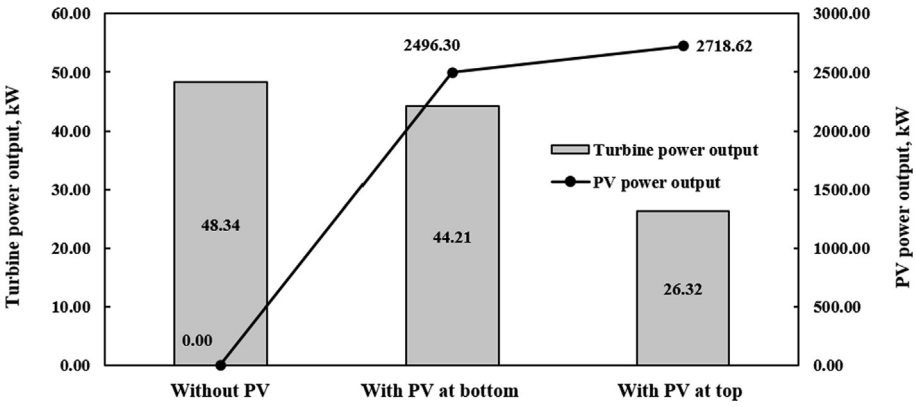

Fig. 10. Comparison of the turbine power output and PV power output when $L = 40$ m. (Two power outputs are not in the same scale).

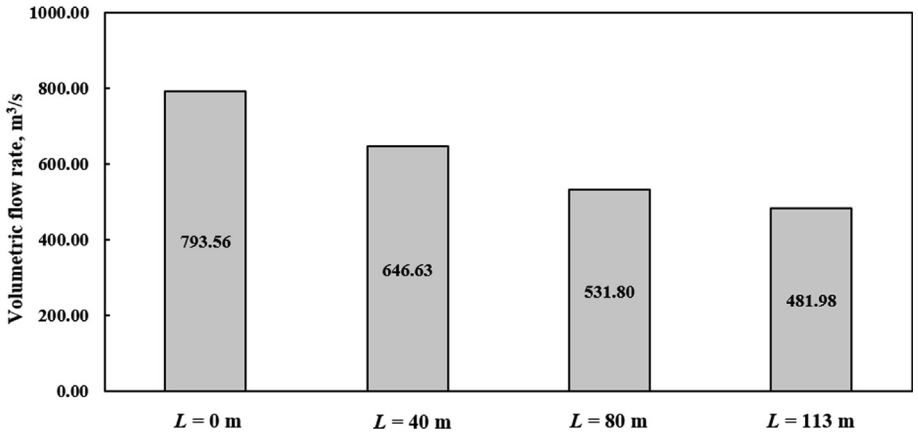

Fig. 11. Comparison of the system thermal volumetric flow rate with different *L*.

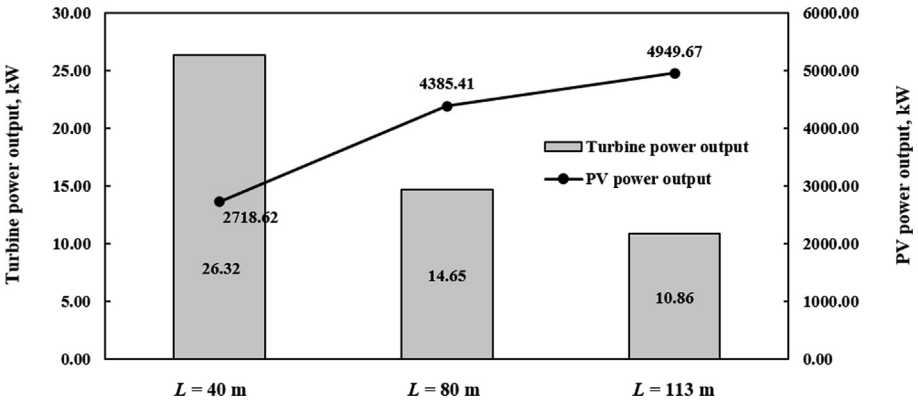

Fig. 12. Comparison of the turbine power output and PV power output with different *L*. (Two power outputs are not in the same scale).

drive suction fans. Ten cases are studied and the results are listed in Table 1.

The air flow rate by the fan can be estimated as follows:

$$\frac{N_{fan}}{N_{ref}} = \frac{Q_{fan}}{Q_{ref}} \tag{23}$$

here N_{fan} is part of the system's generated electricity (by 80%) to drive the suction fan, Q_{fan} is the air flow rate by the suction fan, Q_{ref} is the air flow rate of the pure solar chimney system which is taken as a reference value (793.56 m^3/s at the full-load state and 975.93 m^3/s at the no-load state), andN_{ref} represents the electrical power consumed to produce Q_{ref}. For the full-load state and the no-load state, its values are 2406.05 kW and 3047.96 kW, respectively, computed by the following equation:

$$N = \frac{Q\Delta p}{1000 \times 0.8 \times 0.98} \tag{24}$$

where N is the fan shaft power in kW, Δp is the fan full air pressure drop, and 0.8 and 0.98 in the denominator are ventilator internal efficiency and mechanical efficiency, respectively. Based on the basic principles of fluid mechanics, the air pressure of the solar chimney system was derived by Feng and Yuan [35], as shown in Eq. (25).

$$\Delta p = \frac{1}{2}\rho(v_{out}^2 - v_{in}^2) + (f\frac{l}{d} + \zeta)\frac{\rho v_{out}^2}{2} + \rho g z \tag{25}$$

here v_{in} and v_{out} are the air velocity at the inlet and outlet of the system, d is the chimney equivalent diameter, f *is* the friction coefficient of chimney (taken 0.011) , $\zeta$is the local loss coefficient of chimney bend (taken 1.2) and z denotes the chimney height. In Eq. (25) $\frac{1}{2}\rho(v_{out}^2 - v_{in}^2)$ means the increase in dynamic pressure, $(f\frac{l}{d} + \zeta)\frac{\rho v_{out}^2}{2}$ represents the

Table 1
Electricity production and air flow rate of the solar chimney systems and hybrid systems under full-load condition and no-load condition.

Case	PV position	Width of PV (m)	Load condition	Electricity production by the turbine(kW)	Electricity production by PV panels(kW)	Thermal air flow rate(m^3/s)	Air flow rate by the fan(m^3/s)	Total air flowrate (m^3/s)
1	/	/	full	48.34	0.00	793.56	0.00	793.56
2	/	/	no	0.00	0.00	975.93	0.00	975.93
3	bottom	40	full	44.21	2496.30	770.26	837.91	1608.17
4	bottom	40	no	0.00	2498.72	947.05	800.07	1747.12
7	bottom	113	full	39.05	4520.17	739.08	1503.72	2242.80
8	bottom	113	no	0.00	4538.22	908.75	1453.10	2361.85
5	top	40	full	26.32	2718.62	646.58	905.34	1551.92
6	top	40	no	0.00	2722.62	773.05	871.76	1644.81
9	top	113	full	10.86	4949.67	481.77	1636.08	2117.85
10	top	113	no	0.00	4950.99	576.04	1585.26	2161.30

chimney resistance loss and the local loss into the bend and $\rho gz$is the potential energy increment.

From Table 1, following three important features may be found: First without PV panels the system total air flow rate under no-load condition is above 20% higher than that under full-load condition. However, with PV panels this difference reduces to less than 10%. Second, with PV panels even though the thermal air flow rate reduces a bit, but the total air flow rate, including thermal and fan-driven, is greatly enhanced. For example, when the top of the collector is fully covered with PV panels that is $L = 113$ m, the total air flow rate is 2.21 times of the corresponding solar chimney air flow rate under no-load condition. Third, when PV panels are put at bottom of the collector, the total airflow rate increases the most at same other condition. For $L = 113$ m, the total air flow rate is 2.42 times of the corresponding solar chimney air flow rate under no-load condition. So, the hybrid system applied to the solar-assisted air cleaning system is a good improvement for increasing the air flow rate or decreasing the land requirement for the same flow rate.

It is interesting to see how the PV panel temperature change radially in the collector. Taking Case 9 as an example, the PV panel temperature distribution along the collector radius is illustrated in Fig. 13. Surface temperatures of PV panels near the collector inlet have the lowest values due to cooling by the cold air from the ambient. Along the radius direction towards the collector center, surface temperatures increase, but the highest temperature is only about 50 °C, which is still a good condition for PV panels. From this result it can be seen that the air flow within the collector can cool PV panels effectively hence it increases the panel efficiency.

Finally, it is to be noted that for the large-scale Manzanares pilot power plant, we do not consider the commercially available panels in the market. Hence the type of panels is not specified and their dimensions simply follow the shape and area of the collector.

5. Conclusions

Based on the experimental and numerical investigations presented in the paper, the main conclusions can be drawn as follows:

(1) Small-scale indoor experiments show that the hybrid system, which replace 50.60% acrylic glass with photovoltaic panels, decreases volumetric flow rate by only 14% than the pure solar chimney system.
(2) The comparison between experimental results and numerical simulation results shows that the numerical simulation model developed in this paper, which consists of solar ray tracing model, surface to surface radiation model, buoyancy-driven flow and heat transfer model and power generation model, is reliable.
(3) In the fluid flow and heat transfer simulation, the electricity generated by photovoltaic panels can be treated as a negative heat source to keep the total energy balance of the photovoltaic panels.
(4) For the large-scale system, covering 40-meter-wide photovoltaic panels at the collector bottom and top would reduce the thermal volumetric flow rate by 3% and 19%, respectively, but increase the total power output to 53 times and 57 times, respectively. Panels at the top of the collector has better heat dissipation.
(5) As the photovoltaic panel area increases, the thermal volumetric flow rate decreases but the total power generation increases greatly. Covering the whole top surface of the collector with photovoltaic panels (113-meter-wide) would reduce the thermal volumetric flow rate by only 39.29%, but increase the total power output to 103 times.
(6) The total air flow rate can be increased by using a fan driven by the electric energy generated by the hybrid system. The hybrid system without wind turbine produces more air input. For $L = 113$ m the total air flow rate will increase to 2.42 times with photovoltaic panels at the collector bottom and increase to 2.21 times with photovoltaic panels at the collector top. Thus, covering the collector top by photovoltaic panels or setting the panels on the bottom of collector can greatly improve the utilization of solar energy, resulting in increased air flow rate or decreased land requirement of the solar-assisted air cleaning system.

CRediT authorship contribution statement

Ming-Hua Huang: Conceptualization, Methodology, Software, Investigation, Writing - original draft. **Lei Chen:** Conceptualization. **Le Lei:** Investigation. **Peng He:** Investigation. **Jun-Ji Cao:** Writing - review & editing. **Ya-Ling He:** Writing - review & editing. **Zhen-Ping Feng:** Writing - review & editing. **Wen-Quan Tao:** Formal analysis, Writing - review & editing, Supervision.

Declaration of Competing Interest

The authors declare that they have no known competing financial interests or personal relationships that could have appeared to influence the work reported in this paper.

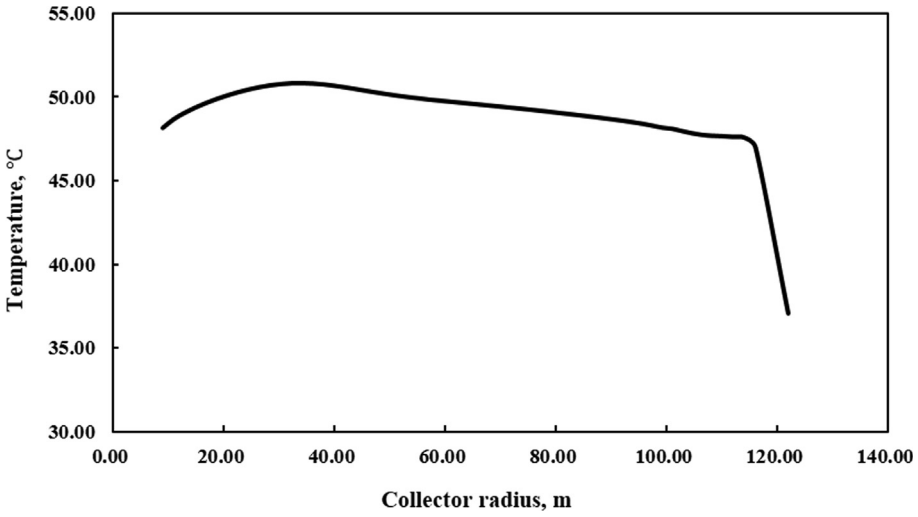

Fig. 13. The PV panel temperature distribution along the collector radius ($L = 113$ m) for Case 9.

Acknowledgements

The authors would like to acknowledge the support provided by the Key Research Program of the Chinese Academy of Sciences (Approved on 8 August, 2014), The Foundation for Innovative Research Groups of the National Natural Science Foundation of China (No. 51721004), and the 111 Project (B16038).

References

[1] IEA. World Energy Outlook Special Report, International Energy Agency. Paris, 2016.
[2] Cao Q, Pui DYH, Lipiński W. A Concept of a Novel Solar-Assisted Large-Scale Cleaning System (SALSCS) for Urban Air Remediation. Aerosol Air Qual Res 2015;15:1–10.
[3] Cyranoski D. China tests giant air cleaner to combat urban smog. Nature 2018;555:152–3.
[4] Haaf W, Friedrich K, Mayr G, Schlaich J. Solar chimneys. Part I: Principle and construction of the pilot plant in Manzanares. Int J Sust Energy 1983;2:3–20.
[5] Haaf W. Solar chimneys. Part II: Preliminary test results from the Manzanares pilot plant. Int. J. Sust. Energy 1984;2:141–61.
[6] Zhou X, Wang F, Ochieng RM. A review of solar chimney power technology. Renew Sustain Energy Rev 2010;14:2315–38.
[7] Gholamalizadeh E, Mansouri SH. A comprehensive approach to design and improve a solar chimney power plant: A special case – Kerman project. Appl. Energy 2013;102:975–82.
[8] Kasaeian AB, Molana S, Rahmani K, Wen D. A review on solar chimney systems. Renew Sustain Energy Rev 2017;67(954–987):4.
[9] Peter N, Kabu OE, Stephen K, Anthony D. 3D finite element method modeling and simulation of the temperature of crystalline photovoltaic module. Int J Res Eng Technol 2015;04:378–84.
[10] Radziemska E. Thermal performance of Si and GaAs based solar cells and modules: a review. Prog Energy Combust Sci 2013;29:407–24.
[11] Skoplaki E, Palyyos JA. On the temperature dependence of photovoltaic module electrical performance: a review of efficiency/power correlations. Sol. Energy 2009;83:614–24.
[12] Tonui JK, Tripanagnostopoulos Y. Improved PV/T solar collectors with heat extraction by forced or natural air circulation. Renew Energy 2007;32:623–37.
[13] Huang BJ, Lin TH, Hung WC, Sun FS. Performance evaluation of solar photovoltaic/thermal systems. Sol Energy 2001;70:443–8.
[14] Chow TT. A review on photovoltaic/thermal hybrid solar technology. Appl Energy 2010;87(2):365–79.
[15] Pastohr H, Kornadt O, Gürlebeck K. Numerical and analytical calculations of the temperature and flow field in the upwind power plant. Int J Energy Res 2004;28:495–510.
[16] Xu G, Ming T, Pan Y, Meng F, Zhou C. Numerical analysis on the performance of solar chimney power plant system. Energy Convers Manage 2011;52:876–83.
[17] Sangi R, Amidpour M, Hosseinizadeh B. Modeling and numerical simulation of solar chimney power plants. Sol Energy 2011;85:829–38.
[18] Cao F, Zhao L, Li H, Guo L. Performance analysis of conventional and sloped solar chimney power plants in China. Appl Therm Eng 2013;50:582–92.
[19] Shen W, Ming T, Ding Y, Wu Y. de-Richter R.K. Numerical analysis on an industrial-scaled solar updraft power plant system with ambient crosswind. Renew Energy 2014;68:662–76.
[20] Gholamalizadeh E, Kim MH. Three-dimensional CFD analysis for simulating the greenhouse effect in solar chimney power plants using a two-band radiation model. Renew Energy 2014;63:498–506.
[21] Guo PH, Li JY, Wang Y. Numerical simulations of solar chimney power plant with radiation model. Renew Energy 2014;62:24–30.
[22] Huang MH, Chen L, He YL, Cao JJ, Tao WQ. A two-dimensional simulation method of the solar chimney power plant with a new radiation model for the collector. Int Commun Heat Mass Transf 2017;85:100–6.
[23] Huang MH, Chen L, He YL, Tao WQ. CFD analysis for the solar chimney power plant combined convection and radiation heat transfer. Busan: The Asian Symposium on Computational Heat Transfer and Fluid Flow; 2015.
[24] Huang MH, He P, Lei L, Tao WQ. A novel solar chimney and photovoltaic hybird power generation system. Chennai: The Asian Symposium on Computational Heat Transfer and Fluid Flow; 2017.
[25] Yang SM, Tao WQ. Heat transfer. 4th ed. Beijing: Higher Education Press; 2006. p. page 377.
[26] Herrando M, Markides CN, Hellgardt K. A UK-based assessment of hybrid PV and solar-thermal systems for domestic heating and power: System performance. Appl. Energy 2014;122:288–309.
[27] Herrando M, Ramos A, Zabalza I, Markides CN. A comprehensive assessment of alternative absorber-exchanger designs for hybrid PVT-water collectors. Appl Energy 2019;235:1583–602.
[28] Notton G, Cristofari C, Mattei M, Poggi P. Modelling of a double-glass photovoltaic module using finite differences. Appl Therm Eng 2005;25:2854–77.
[29] ANSYS, ANSYS FLUENT 14.0 Theory Guide. ANSYS, Inc., 2014.
[30] Tao WQ. Numerical Heat Transfer. 2nd ed., Xi'an, China: Xi'an Jiaotong University Press; 2001.
[31] Gray DD, Giorgin A. The validity of the Boussinesq approximation for liquids and gases. Int J Heat Mass Transfer 1976;19:545–51.
[32] Heo YG, Choi NJ, Choi KH, Ji HS, Kim KC. CFD study on aerodynamic power output of a 110kW building augmented wind turbine. Energy Build 2016;129:162–73.
[33] Li QS, Chen FB, Li YG, Lee YY. Implementing wind turbines in a tall building for power generation: a study of wind loads and wind speed amplifications. J Wind Eng Ind Aerodyn 2013;116:70–82.
[34] Guo J, Lin S, Bilbao JI, White SD, Sproul AB. A review of photovoltaic thermal (PV/T) heat utilization with low temperature desiccant cooling and dehumidification. Renew Sustain Energy Rev 2017;67:1–14.
[35] Feng ZP, Yuan Q. Personal communication; 2015-07.